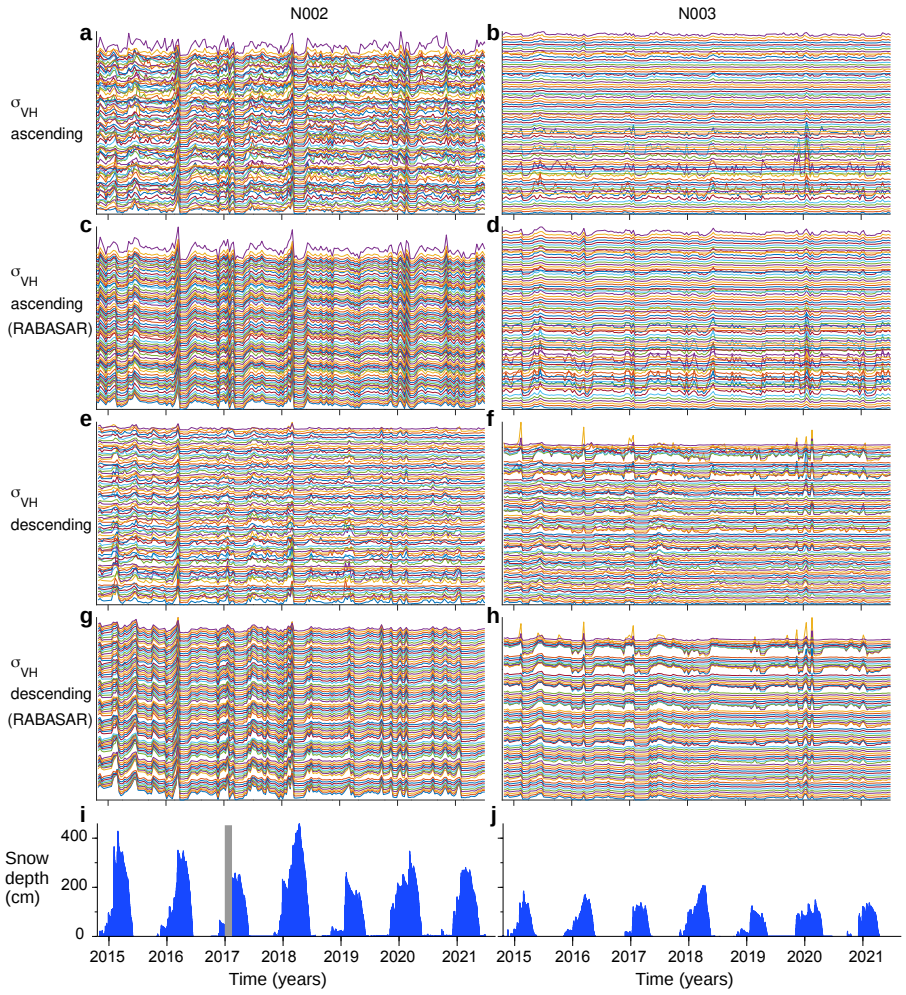

Figure S1: Time series of σ_{VH} at two square grids of 9×9 pixels each, centered on stations N002 and N003 respectively. Panels (**c**), (**d**), (**g**), and (**h**) have been obtained after applying RABASAR to SAR images, in order to lower speckle noise and make plots more readable. All plots have been arbitrarily shifted along the y–axis for clearness. (**a**), (**c**) Pixels nearby N002, ascending orbit. (**b**), (**d**) Pixels nearby N003, ascending orbit. (**e**), (**g**) Pixels nearby N002, descending orbit. (**f**), (**h**) Pixels nearby N003, descending orbit. (**i**) Snow depth at N002, daily data; the gray rectangle indicates lacks of measurements. (**j**) Snow depth at N003, daily data.

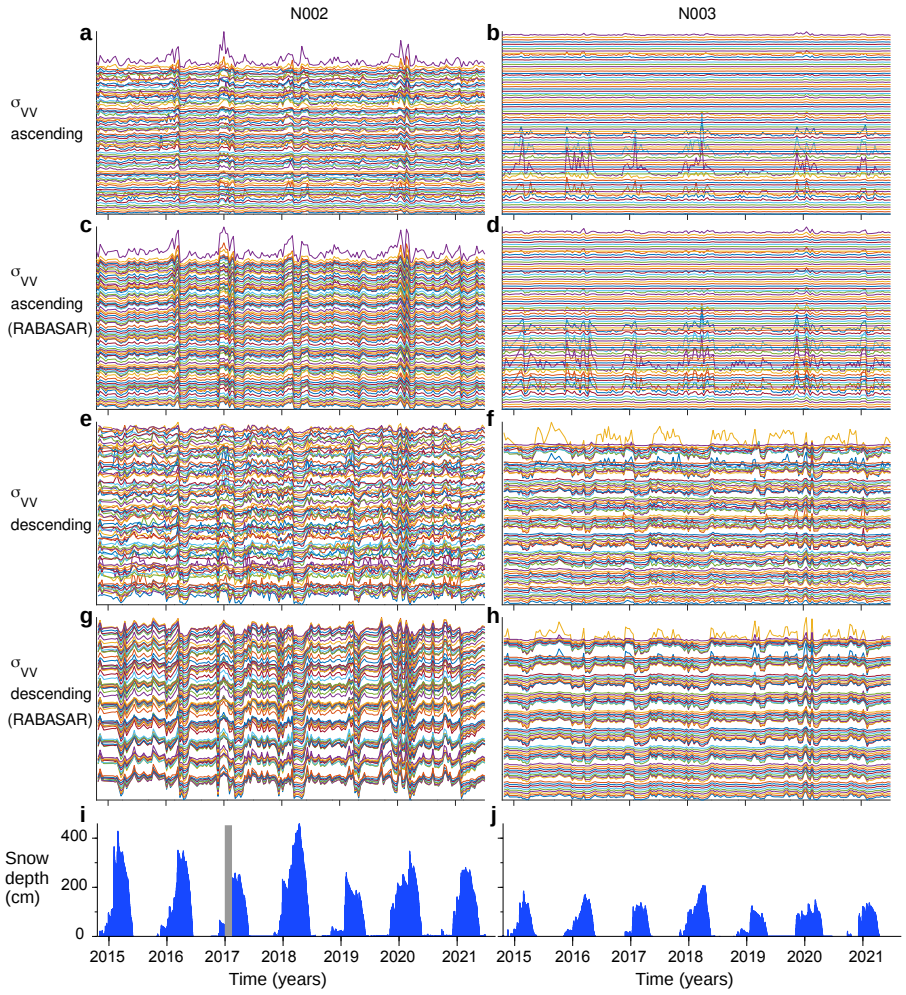

Figure S2: Time series of σ_{VV} at two square grids of 9×9 pixels each, centered on stations N002 and N003 respectively. Panels (**c**), (**d**), (**g**), and (**h**) have been obtained after applying RABASAR to SAR images, in order to lower speckle noise and make plots more readable. All plots have been arbitrarily shifted along the y–axis for clearness. (**a**), (**c**) Pixels nearby N002, ascending orbit. (**b**), (**d**) Pixels nearby N003, ascending orbit. (**e**), (**g**) Pixels nearby N002, descending orbit. (**f**), (**h**) Pixels nearby N003, descending orbit. (**i**) Snow depth at N002, daily data; the gray rectangle indicates lacks of measurements. (**j**) Snow depth at N003, daily data.

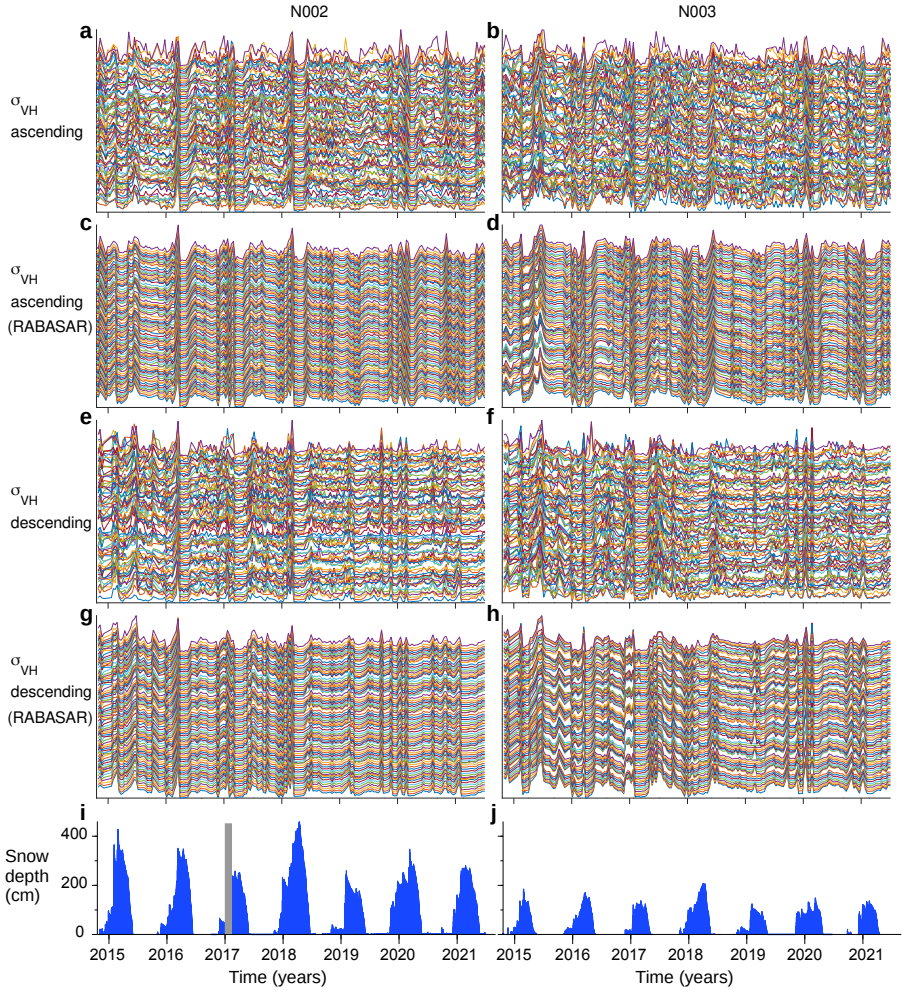

Figure S3: Normalized time series of σ_{VH} at two square grids of 9×9 pixels each, centered on stations N002 and N003 respectively. Normalization evidences common paths among backscattering time series. Panels (**c**), (**d**), (**g**), and (**h**) have been obtained after applying RABASARto SAR images, in order to lower speckle noise and make plots more readable. All plots have been arbitrarily shifted along the y–axis for clearness. (**a**), (**c**) Pixels nearby N002, ascending orbit. (**b**), (**d**) Pixels nearby N003, ascending orbit. (**e**), (**g**) Pixels nearby N002, descending orbit. (**f**), (**h**) Pixels nearby N003, descending orbit. (**i**) Snow depth at N002, daily data; the gray rectangle indicates lacks of measurements. (**j**) Snow depth at N003, daily data.

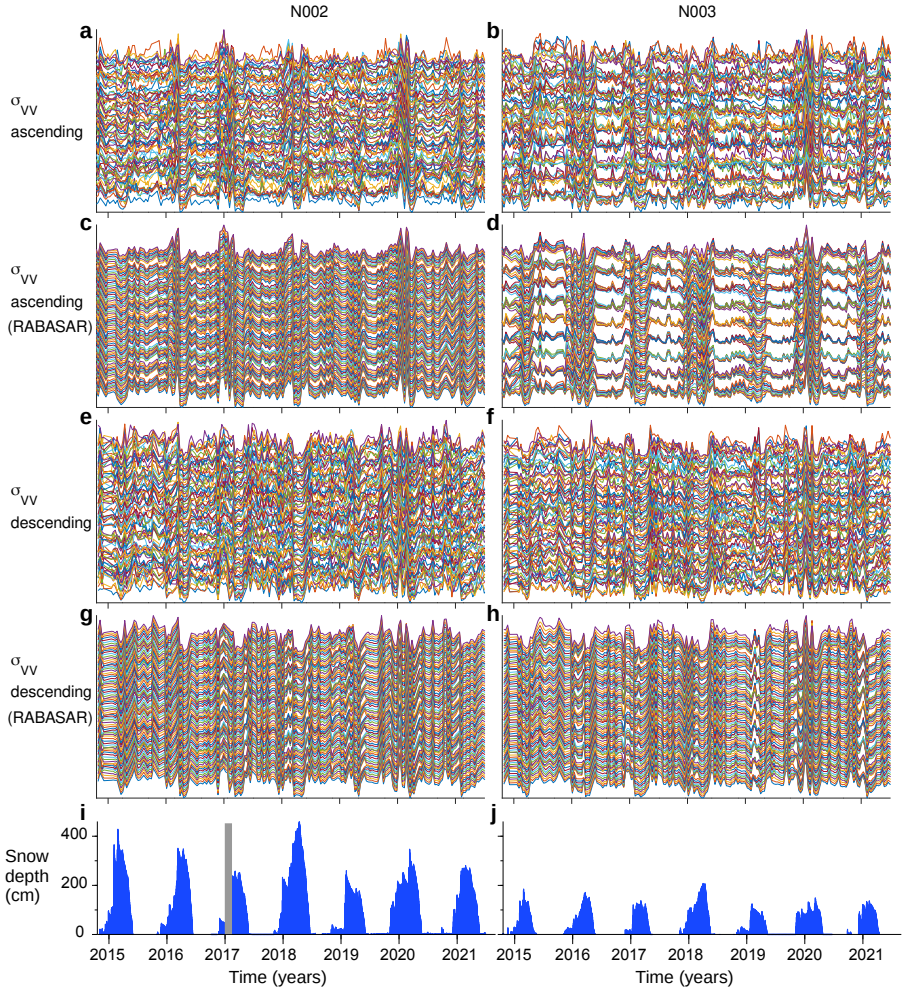

Figure S4: Normalized time series of σ_{VV} at two square grids of 9×9 pixels each, centered on stations N002 and N003 respectively. Normalization evidences common paths among backscattering time series. Panels (**c**), (**d**), (**g**), and (**h**) have been obtained after applying RABASARto SAR images, in order to lower speckle noise and make plots more readable. All plots have been arbitrarily shifted along the y–axis for clearness. (**a**), (**c**) Pixels nearby N002, ascending orbit. (**b**), (**d**) Pixels nearby N003, ascending orbit. (**e**), (**g**) Pixels nearby N002, descending orbit. (**f**), (**h**) Pixels nearby N003, descending orbit. (**i**) Snow depth at N002, daily data; the gray rectangle indicates lacks of measurements. (**j**) Snow depth at N003, daily data.

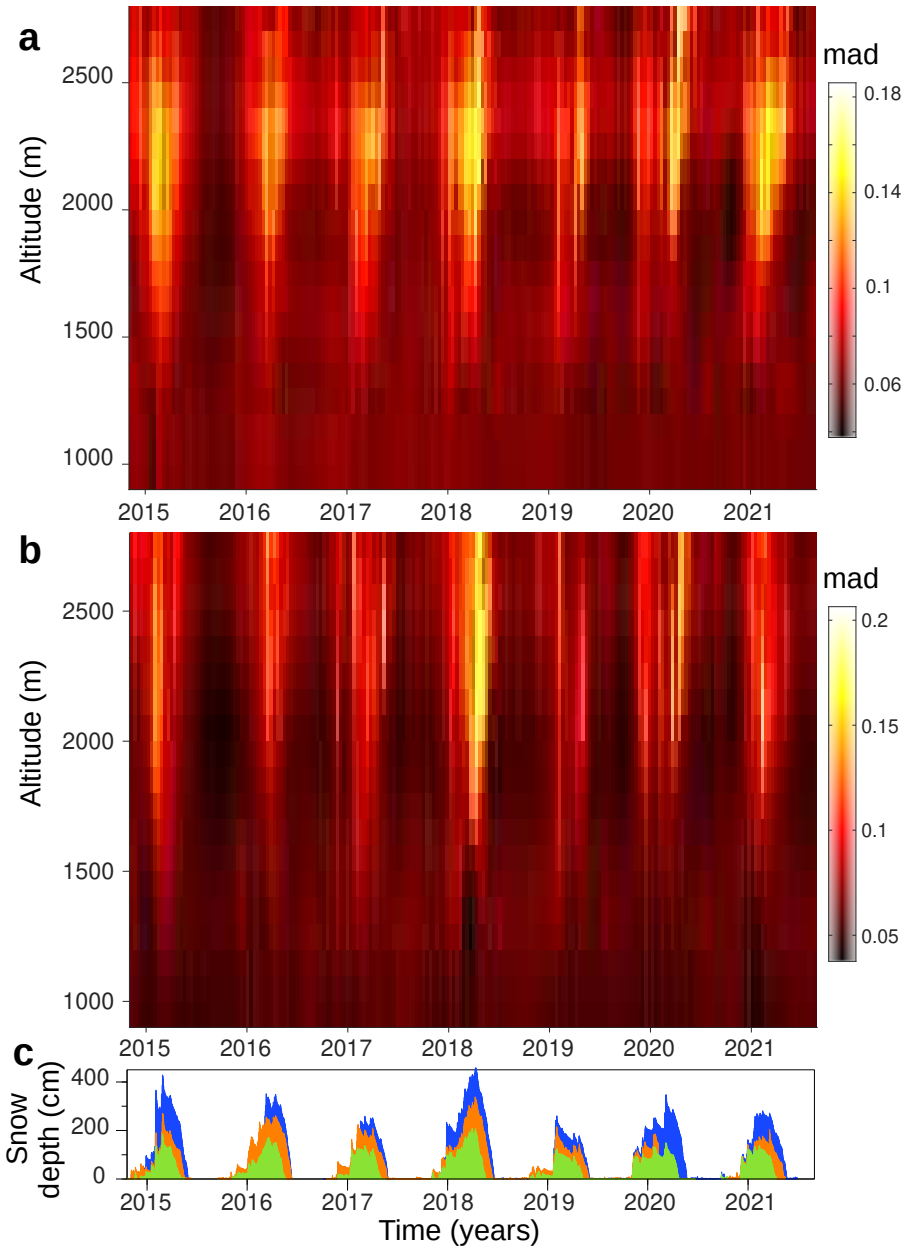

Figure S5: Temporal evolution of the spatial mean absolute deviation of σ_{VH}/σ_{VV} at different altitudes. Altitude ranges 900–2800 m, at 100-m large intervals. (**a**) Ascending orbit. (**b**) Descending orbit. For comparison, (**c**) gives snow depth (daily data) at stations N002 (blue), N003 (green), and N004 (orange).